Letters

Series-Connected Current Source Inverters With Less Switches

Ling Xing and Qiang Wei

***Abstract*—Existing series-connected current source inverters (SC-CSIs) are constructed by identical CSIs connected in series, which involve the use of a high number of switches. In this letter, a new topology with less switches is proposed, and to enable its operation, a new modulation scheme as well as a unique transformer configuration is developed. Lab-scaled experiments are provided to verify the performance of the proposed SC-CSIs.**

***Index Terms*—Modulation, series-connected current source inverters.**

I. Introduction

THE pulsewidth modulation (PWM) current source inverter (CSI) with simple structure, grid-friendly waveform, controllable power factor, and reliable short-circuit protection is well used in medium-voltage drives [1]–[6] and also be considered a good candidate for energy storage system [7], microgrids [8]–[10], and renewable energies [11]–[15]. To enable the application of the CSI in applications with higher power ratings as well as high dc voltage levels, a few identical CSIs are connected in series to form series-connected CSIs (SC-CSIs) as shown in Fig. 1 [13]–[15].

Shown in Fig. 1, the SC-CSIs serve as a centralized dc/ac inverter and are connected to the load through multiwinding transformers. The multiwinding transformers have two functions: one is to provide separate current path for each CSI, and the other to step up the voltage if needed. The voltage/current/power ratings of the transformers are depending on the rating of each CSI and the number of CSIs [13]–[15]. All the employed CSIs are identical in terms of topology, modulation, and control. Assume six switches are used for each constitute CSI, the total number of switches required in the conventional SC-CSIs composed of n CSIs is $6n$.

To lower the number of switches without compromising the other performance of the conventional SC-CSIs, a new topology employing less switches is proposed in this work. The operation principle of the newly proposed SC-CSIs is thoroughly analyzed and presented, based on which a new modulation scheme together with a new configuration of the multiwinding transformer is proposed to ensure proper operation of the proposed inverter.

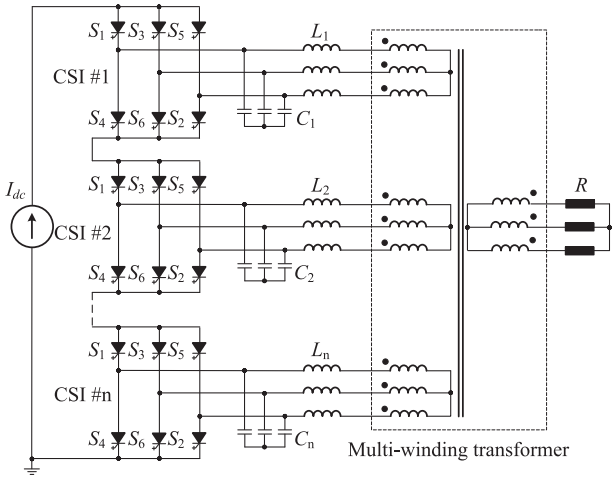

Fig. 1. Conventional SC-CSIs [13]–[15].

II. Proposed SC-CSIs

The proposed SC-CSIs are shown in Fig. 2, in which each constituent CSI is constructed with six switches and the adjacent two CSIs share three switches. By such an arrangement, the number of switches is reduced from $6n$ ($n \geq 2$) in the conventional topology to $3(n+1)$. For example, shown in Fig. 2, the switches S_{11}, S_{12}, S_{13}, S_{21}, S_{22}, and S_{23} form CSI #1 and S_{21}, S_{22}, S_{23}, S_{31}, S_{32}, and S_{33} constitute CSI #2. The design of filters L_n and C_n is same as that of conventional SC-CSIs where $L_1 = L_2 = L_n$ and $C_1 = C_2 = C_n$ and the design of L_n and C_n has been extensively reported in the literature [1], [16], thus not repeated here.

A. Modulation

There are mainly three types of modulation schemes for conventional CSI: space vector modulation (SVM); selected harmonic elimination; and trapezoidal PWM [1]. In this work, an SVM-based modulation scheme is proposed as an example for the proposed SC-CSIs. Fig. 3 shows the space vector diagram for the conventional CSI illustrated in Fig. 1 [1]. The implementation of modulation of CSI requires that at any instant

Manuscript received September 18, 2019; revised October 14, 2019; accepted October 30, 2019. Date of publication November 5, 2019; date of current version February 20, 2020. *(Corresponding author: Qiang Wei.)*

L. Xing is with Thunder Bay, ON P7B 5E1, Canada (e-mail: kaierxing2006@126.com).

Q. Wei is with the Department of Electrical Engineering, Lakehead University, Thunder Bay, ON P7B 5E1, Canada (e-mail: qwei@lakeheadu.ca).

Color versions of one or more of the figures in this letter are available online at http://ieeexplore.ieee.org.

Digital Object Identifier 10.1109/TPEL.2019.2951794

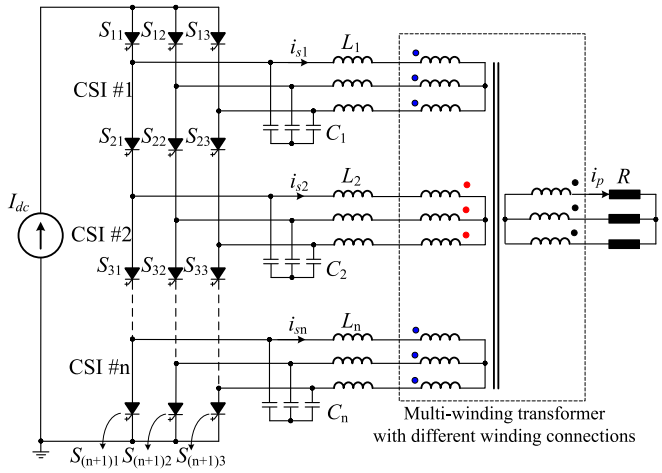

Fig. 2. Proposed SC-CSIs with less switches.

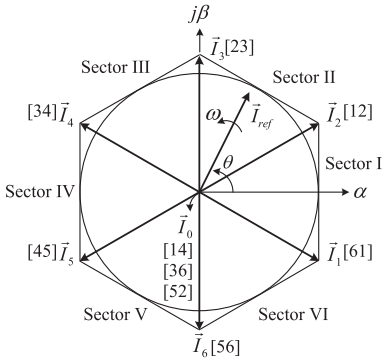

Fig. 3. Space vector diagram of the conventional CSI [1].

(commutation intervals excluded) there are two switches conducting: one in the top and the other in the bottom. For example, shown in the space vector diagram, the on-state switches under the application of Vector I1 (corresponding to the switching state of [61]) are S1 and S6. Please refer to [1] for more details in this regard.

The modulation scheme of the proposed SC-CSIs is developed as follows. First, the modulation scheme of each CSI #m (m = 1, 2, …, n) in the proposed SC-CSIs is same as that of the conventional CSI shown in Fig. 1. The top three switches (S_{m1}, S_{m2}, and S_{m3}) of CSI #m in the proposed topology correspond to S_1, S_3, S_5 in the conventional CSI; and the bottom three ($S_{(m+1)1}$, $S_{(m+1)2}$, and $S_{(m+1)3}$) in the proposed topology correspond to S_4, S_6, S_2 in the conventional CSI, respectively. Second, a special arrangement is developed for the shared three switches of any adjacent two CSIs in the proposed SC-CSIs to ensure proper operation. In the case of CSI #($2m-1$), the switches $S_{(2m)1}$, $S_{(2m)2}$, and $S_{(2m)3}$ function as bottom switches and correspond to S_4, S_6, S_2, whereas in the case of CSI #($2m$), they function as top switches and correspond to S_1, S_3, S_5. Third, the switching states of the shared switches ($S_{(2m)1}$, $S_{(2m)2}$, and $S_{(2m)3}$) are determined by CSI #($2m-1$). Finally, the switching scheme of the proposed SC-CSIs is generated by combining the above all as follows.

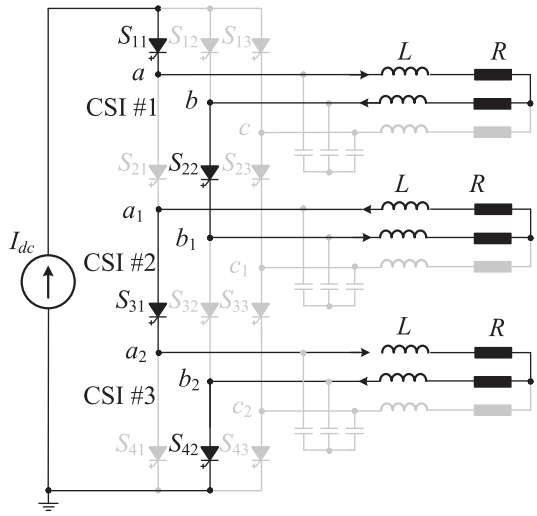

Fig. 4. Equivalent circuit of the proposed SC-CSIs under one switching state.

TABLE I
PROPOSED MODULATION

Modulation (conventional CSI)	S_1, S_3, S_5, S_2, S_6, S_4 [1]
Modulation (proposed SC-CSIs) m = 1, 2, … n	$S_{11} = S_{31} = \ldots = S_{(2m-1)1} = S_1$ $S_{12} = S_{32} = \ldots = S_{(2m-1)2} = S_3$ $S_{13} = S_{33} = \ldots = S_{(2m-1)3} = S_5$ $S_{21} = S_{41} = \ldots = S_{(2m)1} = S_4$ $S_{22} = S_{42} = \ldots = S_{(2m)2} = S_6$ $S_{23} = S_{43} = \ldots = S_{(2m)3} = S_2$
Currents before transformer	$i_{s1} = -i_{s2} = i_{s3} = \ldots = (-1)^{(m+1)} i_{s(m)}$
Current after transformer	$i_{s1} = i_{s2} = i_{s3} = \ldots = i_{s(m)}$
Transformer connections	A phase shift of 180° for CSI #(2 m)

1) The defined output current is ensured with the proposed modulation scheme.
2) A phase shift of 180° exists between the output currents of any two adjacent CSIs.
3) At any instant (commutation excluded), there is a total of ($n+1$) switches being on for the SC-CSIs involving n CSIs and 3($n+1$) switches.
4) The switching frequency of each switch remains the same as that in conventional CSI.

For example, as shown in Fig. 4, assuming the CSI #1 is operating under Vector I_1 ([61]) that the switches S_{11} (corresponding to S_1) and S_{22} (corresponding to S_6) are ON; the Vector I_4 ([34]) is applied to CSI #2 that switches S_{22} (corresponding to S_3 instead of S_6) and S_{31} (corresponding to S_4) are conducting and the resultant output current of CSI #2 is lagging that of CSI #1 by 180°; and similarly CSI #3 is under the application of the Vector I_1 ([61]) that S_{31} (corresponding to S_1) and S_{42} (corresponding to S_6) are in conduction. The modulation scheme for the proposed SC-CSIs involving n CSIs is illustrated in Table I.

B. Configuration of Multiwinding Transformers

A phase shift of 180° exits between the output currents of any two adjacent CSIs as analyzed earlier. To cancel the phase shift and enable the currents after the transformers to be in phase, the inverter-side transformer windings are configured differently. As

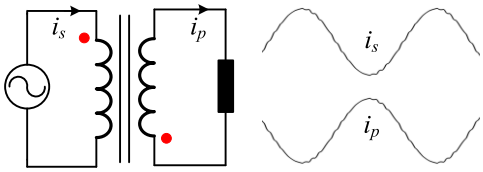

Fig. 5. Per-phase equivalent circuit of reversely dotted transformer.

shown in Fig. 2, the windings for CSI # ($2m$) are reversely dotted compared with those for CSI # ($2m-1$). By doing so, a phase shift of –180° will be generated, which can be seen from its per-phase equivalent circuit of the transformer shown in Fig. 5. Note that this is one of the transformer fundamentals, which can be found in any textbooks regarding transformers, thus not repeated here. The resultant currents of CSI #n after the transformers are therefore in phase. Also, it is worth noting that there is no difference between the transformers in the proposed topology and in the conventional one except the winding connections.

C. Voltage and Current Stress

Like conventional SC-CSIs shown in Fig. 1, all the switches in the proposed SC-CSIs, share an identical current, that is the dc-link current I_{dc} while conducting. Unlike conventional SC-CSIs where all the switches have a same voltage stress, that is the output line-to-line voltage, the switches in the proposed topology have different voltage stresses. The voltage stress of switches in the first and last rows (S_{11}, S_{12}, S_{13} and $S_{(n+1)1}$, $S_{(n+1)2}$, $S_{(n+1)3}$) is same as that in conventional topology, whereas it is doubled for the inner switches under the proposed modulation scheme. Take the equivalent circuit under a given switching state shown in Fig. 4 as an example, the voltage stress for S_{12} is V_{ab}, whereas it is $V_{ab}+V_{b1a1}=2V_{ab}$ for S_{21}. Note that $V_{ab}=V_{b1a1}$ is due to the existence of the 180° phase shift generated by the proposed modulation, which is already analyzed earlier, thus not repeated here.

The switching loss (P_{sw}) and conduction loss (P_{cn}) for switches are calculated as follows [17]:

$$P_{sw}=f_{sw}E_{SR}\left(\frac{i}{I_{nom}}\right)\left(\frac{v}{V_{nom}}\right) \tag{1}$$

$$P_{cn}=(v_{CE0}+r\cdot i)\cdot i \tag{2}$$

where E_{SR} is the rated switching energy, f_{sw} is the switching frequency, I_{nom} and V_{nom} are the rated current and voltage, respectively, i and v are the instant values during switching/conducting, v_{CE0} and r are values to calculate the on-state voltage of the device.

Compared with the conventional topology, the switching losses and conduction losses for switches in the first and last row of the proposed topology remain the same as they share same voltage and current stresses; the total switching losses of the inner switches also remain the same because: 1) though the voltage stress of each inner switch in the proposed topology is twice of that in the conventional one, the number of inner switches is halved; and 2) they share a same current; and the total conduction losses of inner switches in the proposed topology could see a decrease because: 1) they share same conducting current; 2) half switches are conducting; and 3) the saturation voltage v_{CE} for switches with doubled voltage ratings is not doubled as well. For example, v_{CE} is ranging from 1.95 to 2.1 V for 1700 V IGBT, 2.5 to 3.4 V for 3300 V IGBT, and 3 to 4 V for 6600 V IGBT [18]. The same conclusion also applies to other types of power switches and power diode. To sum up, thanks to the contribution of reduced conduction losses, the power losses associated with switches in the proposed topology are less than that in the conventional topology. However, we have to say that how much power loss reduction the proposed topology is able to achieve depends on the developed/used modulation scheme, operation range, selection of switches used to form CSI, power/voltage ratings, etc., and is out of the scope of this letter.

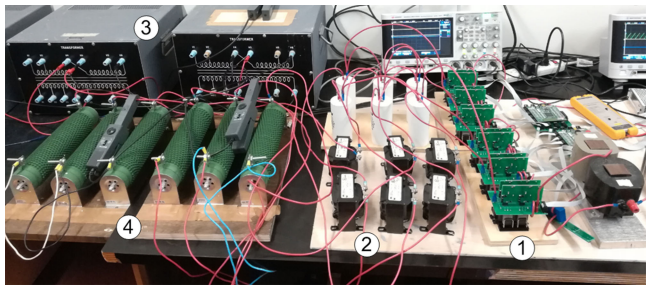

Fig. 6. Photo of experimental setup. 1) SC-CSIs. 2) Filter. 3) Multiwinding transformers. 4) Load.

TABLE II
EXPERIMENT PARAMETERS

DC Current	I_{dc} = 5A
Output Currents	$i_{s1}=i_{s2}$ = 3A
Number of CSIs	2
Switching Frequency	540 Hz
Filter Capacitors	$C_1=C_2$ = 100 μF (0.38 pu)
Filter Inductors	$L_1=L_2$ = 5 mH (0.18 pu)
Resistors	$R_1=R_2$ = 10 Ω

III. EXPERIMENTAL INVESTIGATION

To demonstrate the performance of the proposed SC-CSI and modulation, a lab-scaled setup consisting of two CSIs connected to separate loads (R_1 and R_2) through two three-phase transformers is constructed. Each three-phase transformer is constructed by three single-phase transformers. The setup photo is shown in Fig. 6 and parameters used in the experiments are listed in Table II.

Fig. 7 shows the experimental waveforms of the output currents of CSI #1 and CSI #2 under steady state of $I_{dc}=5$ A. i_{s1} and i_{p1} are currents of CSI #1 before and after the transformer and i_{s2} and i_{p2} are currents of CSI #2 before and after the transformer. i_{s1} and i_{s2} are identical in magnitude but with a phase shift of 180°, which proves that the proposed SC-CSIs and the modulation scheme work well under steady state. i_{p1} and i_{p2} are identical in both magnitude and phase angle which proves the previous analysis as well as the effectiveness of the winding connections of the transformers. Fig. 8 shows the experimental waveforms of the output currents of CSI #1 and CSI #2 under a

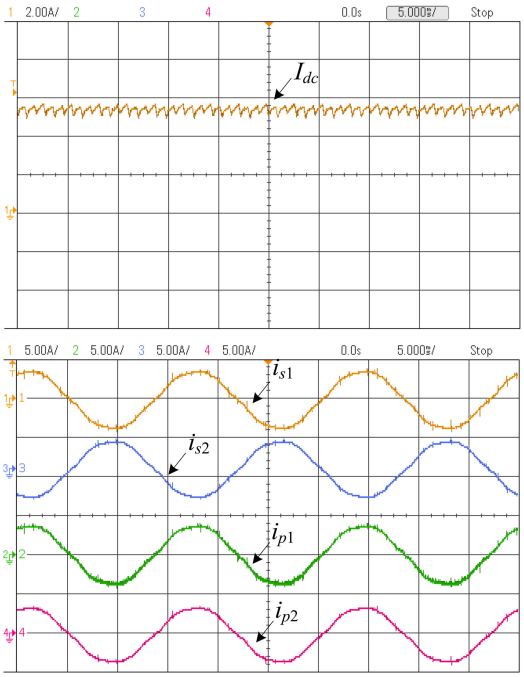

Fig. 7. Experimental waveforms under steady state.

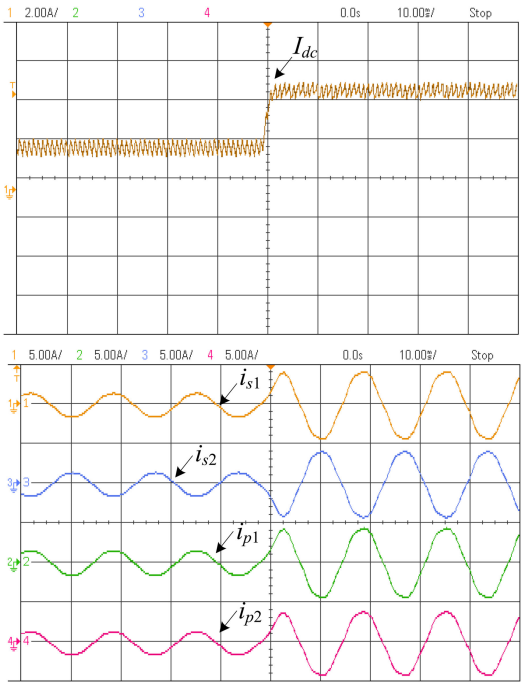

Fig. 8. Experimental waveforms under transient state.

step change of I_{dc} from 2 to 5 A. Similarly, all the currents before and after the transformers follow their respective demand very well and again it verifies that the proposed SC-CSIs, modulation scheme, and configuration of the multiwinding transformers are performing well under transient state.

IV. Conclusion

A new topology of SC-CSIs is proposed. Compared with the conventional one, the proposed one has less switches, lowering the complexity of the inverter significantly and increasing the converter efficiency. To enable its operation, a new modulation scheme is proposed, and on this basis, a unique configuration of the multiwinding transformers is introduced to cancel the generated phase shift in the output currents. The effectiveness of the proposed topology, modulation, and configuration of the transformers are verified based on lab-scaled experiments.

References

[1] B. Wu, *High-Power Converters and AC Drives*. Hoboken, NJ, USA: Wiley, 2006.
[2] Y. W. Li, M. Pande, N. Zargari, and B. Wu, "DC-link current minimization for high-power current-source motor drives," *IEEE Trans. Power Electron.*, vol. 24, no. 1, pp. 232–240, Jan. 2009.
[3] Y. W. Li, M. Pande, N. Zargari, and B. Wu, "Power factor compensation for PWM CSR-CSI fed high power drive system using flux adjustment," *IEEE Trans. Power Electron.*, vol. 24, no. 12, pp. 3014–3019, Dec. 2009.
[4] Z. Wang, B. Wu, D. Xu, and N. R. Zargari, "Hybrid PWM for high-power current-source-inverter-fed drives with low switching frequency," *IEEE Trans. Power Electron.*, vol. 26, no. 6, pp. 1754–1764, Jun. 2011.
[5] J. He, Q. Li, H. Wang, Y. Lyu, H. Jia, and C. Wang, "SVM strategies for simultaneous common-mode voltage reduction and DC current balancing in parallel current source converters," *IEEE Trans. Power Electron.*, vol. 33, no. 10, pp. 8859–8871, Oct. 2018.
[6] Z. Bai, Z. Zhang, and X. Ruan, "A natural soft-commutation PWM scheme for current source converter and its logic implementation," *IEEE Trans. Ind. Electron.*, vol. 58, no. 7, pp. 2772–2779, Jul. 2011.
[7] Z. Wang, B. Yuwen, Y. Lang, and M. Cheng, "Improvement of operating performance for the wind farm with a novel CSC-Type wind turbine-SMES hybrid system," *IEEE Trans. Power Del.*, vol. 28, no. 2, pp. 693–703, Apr. 2013.
[8] X. Guo, D. Xu, J. M. Guerrero, and B. Wu, "Space vector modulation for DC-link current ripple reduction in back-to-back current-source converters for microgrid applications," *IEEE Trans. Ind. Electron.*, vol. 62, no. 10, pp. 6008–6013, Oct. 2015.
[9] X. Guo, Y. Yang, and X. Wang, "Advanced control of grid-connected current source converter under unbalanced grid voltage conditions," *IEEE Trans. Ind. Electron.*, vol. 65, no. 12, pp. 9225–9233, Dec. 2018.
[10] J. He *et al.*, "A fault-tolerant operation approach for grid-tied five-phase current-source converters with one-phase supplying wire broken," *IEEE Trans. Power Electron.*, vol. 34, no. 7, pp. 6200–6218, Jul. 2019.
[11] J. Dai, D. Xu, and B. Wu, "A novel control scheme for current-source converter-based PMSG wind energy conversion systems," *IEEE Trans. Power Electron.*, vol. 24, no. 4, pp. 963–972, Apr. 2009.
[12] S. Anand, S. K. Gundlapalli, and B. G. Fernandes, "Transformer-less grid feeding current source inverter for solar photovoltaic system," *IEEE Trans. Ind. Electron.*, vol. 61, no. 10, pp. 5334–5344, Oct. 2014.
[13] M. Popat, B. Wu, F. Liu, and N. Zargari, "Coordinated control of cascaded current source converter based offshore wind farms," *IEEE Trans. Sustain. Energy*, vol. 3, no. 3, pp. 557–565, Jul. 2012.
[14] Q. Wei, B. Wu, D. Xu, and N. Zargari, "A medium frequency transformer-based wind energy conversion system used for current source converter based offshore wind farm," *IEEE Trans. Power Electron.*, vol. 32, no. 1, pp. 248–259, Jan. 2017.
[15] Q. Wei, B. Wu, D. Xu, and N. R. Zargari, "A new configuration using PWM current source converters in low-voltage turbine-based wind energy conversion systems," *IEEE J. Emerg. Sel. Topics Power Electron.*, vol. 6, no. 2, pp. 919–929, Jun. 2018.
[16] Q. Wei, B. Wu, D. Xu, and N. R. Zargari, "Minimization of filter capacitor for medium-voltage current-source converters based on natural sampling SVM," *IEEE Trans. Power Electron.*, vol. 33, no. 1, pp. 473–481, Jan. 2018.
[17] M. H. Bierhoff and F. W. Fuchs, "Semiconductor losses in voltage source and current source IGBT converters based on analytical derivation," *IEEE 35th Power Electron. Specialists Conf.*, Jun. 2004, vol. 4, pp. 2836–2842.
[18] 2019. [Online]. Available: https://www.infineon.com/cms/en/product/power/igbt/igbt-modules/